Entinostat Enhances the Efficacy of Chemotherapy in Small Cell Lung Cancer Through S-phase Arrest and Decreased Base Excision Repair

Anna Solta[1], Kristiina Boettiger[1], Ildikó Kovács[2], Christian Lang[1,3], Zsolt Megyesfalvi[1,2,4], Franziska Ferk[5], Miroslav Mišík[5], Konrad Hoetzenecker[1], Clemens Aigner[1], Christian R. Kowol[6], Siegfried Knasmueller[5], Michael Grusch[5], Beáta Szeitz[7], Melinda Rezeli[8], Balazs Dome[1,2,4,9], and Karin Schelch[1,5]

ABSTRACT

Purpose: Acquired chemoresistance is a frequent event in small cell lung cancer (SCLC), one of the deadliest human malignancies. Histone deacetylase inhibitors (HDACi) have been shown to synergize with different chemotherapeutic agents including cisplatin. Accordingly, we aimed to investigate the dual targeting of HDAC inhibition and chemotherapy in SCLC.

Experimental Design: The efficacy of HDACi and chemotherapy in SCLC was investigated both *in vitro* and *in vivo*. Synergistic drug interactions were calculated based on the HSA model (Combenefit software). Results from the proteomic analysis were confirmed via ICP-MS, cell-cycle analysis, and comet assays.

Results: Single entinostat- or chemotherapy significantly reduced cell viability in human neuroendocrine SCLC cells. The combination of entinostat with either cisplatin, carboplatin, irinotecan, epirubicin, or etoposide led to strong synergy in a subset of resistant SCLC cells. Combination treatment with entinostat and cisplatin significantly decreased tumor growth *in vivo*. Proteomic analysis comparing the groups of SCLC cell lines with synergistic and additive response patterns indicated alterations in cell-cycle regulation and DNA damage repair. Cell-cycle analysis revealed that cells exhibiting synergistic drug responses displayed a shift from G_1 to S-phase compared with cells showing additive features upon dual treatment. Comet assays demonstrated more DNA damage and decreased base excision repair in SCLC cells more responsive to combination therapy.

Conclusions: In this study, we decipher the molecular processes behind synergistic interactions between chemotherapy and HDAC inhibition. Moreover, we report novel mechanisms to overcome drug resistance in SCLC, which may be relevant to increasing therapeutic success.

Introduction

Small cell lung cancer (SCLC) accounts for approximately 13%–15% of all lung cancers and is still classified as a recalcitrant malignancy ensued from a dismal prognosis (1). Characteristically, rapid tumor growth and early metastasis along with the almost universal inactivation of the tumor suppressor genes *TP53* and *RB1* potentiate the aggressive nature of SCLC (2). Most patients with SCLC are not eligible for surgical resection due to already present metastatic lesions or mediastinal lymph node involvement at the time of initial diagnosis (3). SCLC carcinogenesis is significantly associated with excessive exposure to tobacco carcinogens, resulting in characteristic genetic alterations including a drastic increase in tumor mutational burden (4).

Although emerging evidence from preclinical studies indicates the existence of unique molecular subtypes of SCLC based on the expression profiles of four transcription factors, including achaete-scute homolog 1 (ASCL1), neurogenic differentiation factor 1 (NEUROD1), POU class 2 homeobox 3 (POU2F3), and yes-associated protein 1 (YAP1), the current treatment regimen of SCLC patients does not consider the biological background (5). The standard systemic therapy consists of a platinum compound (either cisplatin or carboplatin) combined with a topoisomerase inhibitor (etoposide or irinotecan; refs. 6–9). Additionally, epirubicin is of therapeutic interest and has been investigated in several clinical trials in SCLC (10).

In contrast to non–small cell lung cancer (NSCLC), where major improvements in personalized therapy have recently been achieved, only a small number of novel therapeutic agents such as immune-checkpoint inhibitors targeting PD-L1 have gained approval for SCLC (11, 12). Although SCLC is initially highly sensitive to standard-of-care cytotoxic agents, acquired therapeutic resistance with the consequence of disease recurrence is a common phenomenon and remains a significant challenge in SCLC patients (9).

Histone deacetylase inhibitors (HDACi) were recently described to display cytotoxic activity in different malignant entities including melanoma (13), acute leukemia (14), and SCLC (15). Five agents with

[1]Department of Thoracic Surgery, Comprehensive Cancer Center, Medical University of Vienna, Vienna, Austria. [2]National Koranyi Institute of Pulmonology, Budapest, Hungary. [3]Division of Pulmonology, Department of Medicine II, Medical University of Vienna, Austria. [4]Department of Thoracic Surgery, Semmelweis University and National Institute of Oncology, Budapest, Hungary. [5]Center for Cancer Research, Medical University Vienna, Vienna, Austria. [6]Institute of Inorganic Chemistry, Faculty of Chemistry, University of Vienna, Vienna, Austria. [7]Division of Oncology, Department of Internal Medicine and Oncology, Semmelweis University, Budapest, Hungary. [8]Department of Biomedical Engineering, Lund University, Lund, Sweden. [9]Department of Translational Medicine, Lund University, Lund, Sweden.

B. Dome and K. Schelch share the senior authorship of this article.

Corresponding Authors: Balazs Dome, Department of Thoracic Surgery, Comprehensive Cancer Center; Medical University of Vienna, Waehringer Guertel 18-20, A-1090, Vienna, Austria. E-mail: balazs.dome@meduniwien.ac.at; and Karin Schelch, Department of Thoracic Surgery, Comprehensive Cancer Center; Medical University of Vienna, Waehringer Guertel 18-20, A-1090, Vienna, Austria. E-mail: karin.schelch@meduniwien.ac.at

Clin Cancer Res 2023;29:4644–59

doi: 10.1158/1078-0432.CCR-23-1795

Translational Relevance

Small cell lung cancer (SCLC) is characterized by rapid disease recurrence and acquired resistance to systemic therapy. In this study, we evaluated the efficacy of the histone deacetylase (HDAC) inhibitor entinostat in combination with clinically relevant chemotherapeutic agents in human SCLC. The vast majority of cell lines demonstrated additive response to dual entinostat and chemotherapy. A synergistic response upon combinational therapy was predominantly seen in cell lines that were resistant to monotherapy. Moreover, cisplatin combined with entinostat demonstrated higher efficacy *in vivo*. Proteomic analysis and experimental validation revealed that distinct cell-cycle checkpoint regulation and concomitant changes in DNA repair are highly associated with these synergistic drug interactions. Altogether, our findings suggest that resistant SCLC cells may benefit from concomitant treatment using entinostat and chemotherapy to overcome drug resistance.

a confirmed HDAC-mediated mechanism of action in various hematologic indications have been approved (including multiple myeloma; ref. 16). Entinostat (MS-275) is currently being tested in clinical trials for the treatment of various malignancies such as breast, lung, bladder, colorectal, and renal cancers (17). Unfortunately, although preclinical results on HDACi have been promising, these agents have only shown moderate success as monotherapy in early-phase clinical trials for NSCLC and prostate cancer (18).

HDACi are commonly proposed to act synergistically with numerous standard chemotherapies in preclinical settings. Mathematical models are, therefore, used to investigate pharmacodynamic interactions, where synergy between two drugs refers to enhanced potential compared with each drug's individual activity. However, the terms synergism, additivity, and antagonism are based on *in silico* models and need further validation in a human pharmacologic context (19). Recent research has focused on the application of HDACi in combination with cytotoxic agents in NSCLC in an effort to increase their efficacy and reduce drug resistance (18, 20). Entinostat, a class I HDAC inhibitor, has been demonstrated to synergize with various other agents such as the epidermal growth factor receptor (EGFR) inhibitor erlotinib or the DNA methyltransferase inhibitor decitabine in NSCLC (21, 22). It remains elusive whether the addition of entinostat to systemic therapy has a direct impact on tumor growth in SCLC.

In this study, we used a stepwise approach testing the potency of the HDACi entinostat on an extended panel of human SCLC cell lines as a single agent followed by a combination with cisplatin and other clinically relevant chemotherapeutic agents. Next, we confirmed the effect of entinostat and cisplatin using a xenograft mouse model. In order to examine the molecular characteristics of SCLC cell lines showing differential responses to therapy and to identify the underlying mechanisms, we reanalyzed our recently published proteomic data set of human SCLC cell lines (23). Overall, the aim of this study was the development of an improved therapeutic strategy for this devastating disease.

Materials and Methods

Cell culture

Commercially available human SCLC cell lines ($N = 16$) as well as the lung adenocarcinoma cell line A549 (RRID:CVCL_0023) were cultured in RPMI-1640 medium (with L-glutamine, Sigma) supplemented with 10% heat-inactivated fetal bovine serum. Cells were maintained in a humidified atmosphere at 37°C and 5% CO_2. Unless stated otherwise, all treatments with inhibitors were started 24 hours after seeding. Cells were purchased from the American Type Culture Collection (ATCC; authenticated by STR profiling) in 2017. All experiments were performed within 15 passages. Cells were tested for *Mycoplasma* contamination once a month (MycoAlert, Lonza).

Proteomic analysis

The proteomic data set used in this study was recently published by our group (23). Briefly, 26 SCLC cell lines were subjected to nLC MS/MS. In this study, the data set was reanalyzed, comparing only the Enti^{sens} (H82, H524, H1694, CLR-L311, and DMS53) with Enti^{res} (H372, H841, H1048, and CRL-2177) cells as well as SYN (H841, H372, H2171, H196, H1048, and SHP77) versus ADD (GLC4, COR-L311, CRL-2177, H1694, H524, and HLHE) groups. Differentially expressed proteins were subjected to ToppCluster analysis ($P \leq 0.05$) and 1D annotation enrichment was done considering all proteins (24). Additionally, gene set enrichment analysis (GSEA, RRID:SCR_003199) was performed using the GSEA software version 4.3.2 (25, 26).

Drug treatment and cell viability assays

Adherent cells and cells in suspension were stained with trypan blue before counting. Live cells ($5–10 \times 10^3$) were seeded in a 96-well plate. On the next day, drug dilutions were prepared and added as indicated. Entinostat (MedChemExpress) was diluted in DMSO and a corresponding vector control was included. Cisplatin, carboplatin, etoposide (all Accord Healthcare), and epirubicin (Teva) were diluted in PBS. Irinotecan (MedChemExpress) was diluted in DMSO. Single drugs as well as combinations were administered for 72 hours. Plates were incubated at 37°C/5% CO_2. MTT solution (EZ4U, Biomedica) was prepared according to the manufacturer's specifications, added to each well, and incubated between 30 minutes and 2 hours. Absorbance was measured at 450 nm and 620 nm (Varioskan Lux; Thermo Fisher Scientific).

Protein isolation and western blots

Cells (5×10^5) were seeded in a 6-well plate. Cells were treated with entinostat (2.5 μmol/L), cisplatin (5 μmol/L), or a combination of both drugs on the following day and harvested 24 hours later in RIPA buffer supplemented with halt proteinase inhibitor cocktail (Thermo Fisher Scientific). Protein content was determined using the Pierce BCA Protein Assay Kit (Thermo Fisher Scientific). Proteins (10 μg unless stated otherwise) were separated by SDS/PAGE and semi-dry blotted onto nitrocellulose membranes. Immunodetection was performed with the Super Signal West Femto Chemiluminescent Substrate (Thermo Fisher Scientific) using primary antibodies against total and cleaved PARP (#9,542, Cell Signaling Technology, RRID:AB_2160739, 1:1,000), γH2AX (SAB5600038, Sigma, 1:1,000), Histone3 (sc517576, Santa Cruz, 1:200), Acetyl-H3 (#9677, Cell Signaling Technology, 1:1,000), and GAPDH (#5174, Cell Signaling Technology, 1:10,000) as loading controls.

Inductive-coupled plasma mass spectrometry (ICP-MS)

For the analysis of the intracellular platinum (Pt) content *in vitro*, cells (2×10^5) were seeded in a 6-well plate in triplicates. After 48 hours of incubation, cisplatin (10 μmol/L) was either added alone or in combination with entinostat (5 μmol/L) for 3 hours. Additionally, cells were exposed to entinostat (1 μmol/L) 24 hours prior to the 3-hour treatment with cisplatin (10 μmol/L). Following drug exposure, cells

were washed twice with PBS and subsequently dissolved in 500 μL HNO_3 (67%–69%, suprapur for trace metal analysis, NORMATOM; VWR). After 1-hour incubation at room temperature, samples were diluted 1:20 in ultrapure water. Meanwhile, cells of two additional wells were counted, and the total cell number was determined for normalization.

For Pt levels *in vivo*, digestion of tumors (approximately 15–30 mg gravimetrically weighted) was performed with 2 mL of approximately 20% HNO_3 and 100 μL H_2O_2 suprapur (Merck, 30%) using an open vessel graphite digestion system (coated graphite heating plate, coated sample holder-top for 25 mL vials, PFA vials and PFA lids; Labter, ODLAB; Distributor: AHF Analysentechnik AG). Pt content was determined using an Agilent 7800 instrument (Agilent Technologies), equipped with an Agilent SPS 4 autosampler (Agilent Technologies) and a MicroMist nebulizer at a sample uptake rate of approximately 0.2 mL/minute. Pt and rhenium standards for ICP-MS measurements were derived from CPI International. The Agilent MassHunter software package (Workstation Software, version C.01.04, Build 544.17, Patch 3, 2018, RRID:SCR_016657) was used for data processing. The experimental parameters for ICP-MS 7800 were as follows: RF power: 1550W; cone material: nickel; carrier gas: 1.08 L/minute; plasma gas: 15 L/minute; monitored isotopes: ^{185}Re, ^{195}Pt, ^{196}Pt; integration time: 0.1 s; number of sweeps: 100; number of replicates: 12. The instrument was tuned daily to achieve maximum sensitivity.

Cell-cycle analysis

Cells (5×10^5) were seeded in 6-well culture plates and incubated overnight at 37°C, 5% CO_2. The following day, cells were treated either with IC_{50} concentrations of entinostat, cisplatin, a combined regimen, or vehicle for 24 hours, respectively. After centrifugation, the supernatants were removed and cell pellets were immediately put on ice. Cells were fixed by adding 1 mL of 70% ethanol (precooled at −20°C) and incubated on ice for 30 minutes. Samples were centrifuged prior to resuspension in 200 μL of propidium iodide (PI) solution (50 μg/mL PI, 500 μg/mL RNAse in PBS). After incubation for 15 minutes at 37°C, the cells were stored on ice until data acquisition by flow cytometry using a DxFlex Flow Cytometer (Beckman Coulter).

Apoptosis assay

Cells (5×10^5) were seeded in a 6-well culture plate and incubated overnight at 37°C. After cell harvesting and centrifugation, cells were resuspended in PBS +/+ (Gibco). After centrifugation, cells were resuspended in 1× annexin-binding buffer containing FITC annexin V (556419; BD Pharmingen) and PI (HY-D0815, MedChemExpress). After 15 minutes of incubation at RT in the dark, data acquisition was performed on a DxFlex Flow Cytometer (Beckman Coulter).

Singe cell gel electrophoresis (comet) assay

These assays were performed according to the international guidelines for single-cell gel electrophoresis (SCGE) experiments (27, 28). Cells (5×10^5) were seeded in a 6-well culture plate and viability was determined using trypan blue before analysis (DNA damage was analyzed only in samples with viability ≥70%). For standard comet assays, cells (2×10^5) were mixed with 0.5% LMPA (UltraPure Low Melting Point Agarose, Invitrogen) and transferred to agarose-coated slides (1.0% normal melting point agarose, SERVA Electrophoresis GmbH). After 1 hour lysis (2.5 M NaCl, 0.1 M Na2EDTA, 10.0 mmol/L Trizma base, pH 10.0, before using, 1% Triton X-100 was freshly added), unwinding (30 minutes) and electrophoresis (30 minutes, 300 mA, 1.0 V/cm, at 4°C) was carried out under alkaline conditions (0.3 M NaOH, 1.0 mmol/L Na2EDTA, pH > 13). Subsequently, the slides were washed twice with dH_2O (8 minutes), air-dried, and stained with PI (10 μg/mL, Sigma-Aldrich). In SCGE experiments under standard conditions, H_2O_2 (50 μmol/L, 5 minutes on ice, Sigma-Aldrich) was used as a positive control. Negative controls were exposed to PBS (Ca and Mg free, PAA Laboratories GmbH).

Nuclei (150) were evaluated randomly per experimental point. Cells were examined under a fluorescence microscope (Nikon EFD-3) using a 20-fold objective. DNA migration was determined by a computer-aided image analysis system (Comet Assay IV, Perceptive Instruments). The percentage of DNA in the tail (% DNA) was measured as an endpoint.

Repair enzyme comet assay

A modification of the SCGE assay was used to measure base excision repair (BER) and nucleotide excision repair (NER; ref. 29). This approach is based on the ability of repair proteins in cell extracts to recognize and cut substrate DNA containing specific lesions that are repaired by different repair enzymes (28). Protein extracts were prepared from 5×10^5 cells by centrifugation ($700 \times g$, 10 minutes, 4°C) after addition of 200 μL of extraction buffer (45 mmol/L HEPES, 0.4 M KCl, 1 mmol/L EDTA, 0.1 mmol/L dithiothreitol, 10% glycerol, pH 7.8) with 1% of Triton X-100 (buffer A). Samples were vortexed at maximum speed and snap-frozen in liquid nitrogen. Lysates were thawed and centrifuged at 15,000 × *g* (5 minutes at 4°C). Supernatants (200 μL) were collected and mixed with 60 μL cold buffer B (40 mmol/L HEPES, 0.5 mmol/L EDTA, 0.2 mg/mL BSA, 0.1 M KCl, pH 8.0). Protein concentrations of extracts were quantified with a Protein Assay Kit (BCA Protein Assay Kit, Pierce).

A549 cells (a human lung fibroblast carcinoma cell line, provided by the ATCC; RRID:CVCL_0023) were used as substrate cells and were cultivated in RPMI-1640 medium (low glucose, with L-glutamine) supplemented with 10% FCS under humidified conditions (37°C, 5% CO_2). Cells were washed with Dulbecco's PBS at 85%–90% confluence and harvested with 0.25% trypsin-EDTA.

As for the BER measurements, the photosensitizer Ro 19-8023 (Chiron AS), which causes oxidation of DNA bases, was used at 1.0 μmol/L. Substrate cells were treated in the presence and absence of visible light (400 W, 60 cm distance, 4 minutes). Subsequently, cells were centrifuged ($700 \times g$ for 10 minutes), and resulting pellets were resuspended in a freezing medium and cryopreserved at −80°C. For NER measurements, UVC (2.0 Jm-2, 0.4 minutes on ice) was used to produce cyclobutane pyrimidine dimers.

Chemically treated substrate cells (2.0×10^4 per gel) were embedded in agarose and lysed (1 hour). For NER measurements, slides were washed twice for 10 minutes in buffer N (45 mmol/L HEPES, 0.25 mmol/L EDTA, 0.3 mg/mL BSA, 2% glycerol, pH 7.8) and buffer B was used for BER (40 mmol/L HEPES, 0.5 mmol/L EDTA, 0.2 mg/mL BSA, 0.1 M KCl, pH 8.0). Subsequently, nuclei were incubated (30 minutes) with either 50 μL "extract mix" (cell extract, extract buffer with Triton X-100, and reaction buffers) or with 50 μL control buffer. FPG (BER experiments) and T4EndoV (NER measurements) were used as positive controls. Negative controls contained buffer B (for BER) and buffer N (for NER). Alkaline unwinding (30 minutes) and electrophoresis (30 minutes) were performed as in standard comet experiments.

In vivo xenograft model

H841 cells (5×10^6) dissolved in serum-free medium were inoculated subcutaneously into 8–10-week old female SCID mice. Upon tumor formation after 21 days, mice were randomly assigned into four

groups (control, entinostat, cisplatin, entinostat + cisplatin, $N = 8$ per group). Entinostat was administered twice a week via oral gavage at 25 mg/kg in 5% DMSO in 10 μL/g corn oil. Cisplatin was injected intraperitoneally once a week at 3 mg/kg. Respective controls were treated with NaCl or DMSO in corn oil. Mice were checked daily for water and food consumption; body weight and tumor size were measured three times a week by using a caliper. Mice were sacrificed after 30 days, one day after the last treatment. All *in vivo* experiments were carried out in accordance with the NIH guidelines for the use of experimental animals and were approved by the Animal Care and Use Committee of the Semmelweis University, Hungary (permission No. PEI/001/2457-6/2015).

Histological analysis of tumors

Xenografts from the *in vivo* experiment were harvested, fresh-frozen, and cryosectioned into 6-μm sections. Sections were fixed using phosphate-buffered 4% formaldehyde and incubated with 0.3% H_2O_2 for 10 minutes. Slides were incubated with primary antibodies against Ki-67 (ab15580, Abcam, RRID:AB_443209, 1:100) and cleaved PARP (#5625, Cell Signaling Technologies, RRID:AB_10699459, 1:50) for 1 hour and with the respective secondary antibodies for 30 minutes. Sections were further developed using 3,3′diaminobenzidine (DAB). The TUNEL reaction was carried out using an *in situ* cell death detection fluorescein kit (Roche) according to the manufacturer's instructions. Nuclei were counterstained with hematoxylin or DAPI for IHC and the TUNEL reaction, respectively. Slides were scanned using SCAN II (3DHistech) and MIDI (3DHistech) for bright field and fluorescence. Six to 20 representative images per group were randomly taken and manually evaluated using ImageJ (RRID:SCR_003070).

Statistical analysis

Unless stated otherwise, all data were statistically analyzed using GraphPad Prism 8.0 (RRID:SCR_002798). Evaluation of the proteomic data was performed using v4.0 (30) and Perseus v1.6 (31). Drug interactions were evaluated using the Combenefit software, which calculates synergism scores based on the mathematical HSA model (32). Negative values define antagonistic, whereas positive values suggest synergistic drug interactions. A value of zero indicates additive effects. In our study, we defined a cutoff of 35 of the maximum synergism score to differentiate between "additive" and "synergistic" activities of the drugs in our cell models. Unless stated otherwise, all data are shown as the mean of at least three independent experiments performed in triplicate. Error bars represent the standard error of the mean (SEM). Differences between two or multiple groups were calculated by Students *t* test and one-way ANOVA combined with Kruskal–Wallis multiple comparisons test, respectively. Correlation analysis was performed using the Anderson–Darling test for normal distribution, and Spearman r was calculated accordingly. Results were considered statistically significant if $P \leq 0.05$ (*), $P < 0.01$ (**), $P < 0.001$ (***).

Data availability statement

All proteomic data used in this study were previously published by Szeitz and colleagues (23). The data generated in this study are available upon request from the corresponding author. The mass spectrometry proteomics data have been deposited to the ProteomeXchange Consortium via the PRIDE 85 partner repository with the data set identifiers PXD029805 and 10.6019/PXD029805 (cell pellet data), PXD029821 and 10.6019/PXD029821 (culture media data). The scripts for the proteomic data analyses can be obtained at: https://github.com/bszeitz/SCLC_proteomics.

Results

SCLC cell lines respond differently to entinostat

To evaluate the *in vitro* efficacy of entinostat, 16 cell lines representing all four molecular SCLC subtypes (SCLC-A, SCLC-N, SCLC-P, and SCLC-Y) were treated with entinostat. The compound dose-dependently decreased cell viability, with IC_{50} values ranging between 0.3 nmol/L and 29.1 μmol/L (calculated from dose–response curves, **Fig. 1A**; Supplementary Fig. S1). Although no molecular subtype showed a significant response to entinostat treatment, SCLC-Y demonstrated a trend toward resistance. However, cell lines with high neuroendocrine (NE) expression patterns (SCLC-A, SCLC-N) were significantly more sensitive to entinostat than cell lines established from nonneuroendocrine SCLC (NNE, SCLC-P, SCLC-Y; **Fig. 1B**).

Next, by defining entinostat IC_{50} thresholds of below 1 μmol/L and above 7 μmol/L, cell lines were grouped as entinostat-sensitive ($Enti^{sens}$, $N = 5$) and entinostat-resistant ($Enti^{res}$, $N = 4$) and compared by using our recently published proteomic data set (23). This analysis revealed 327 and 410 significantly upregulated proteins in the $Enti^{sens}$ and $Enti^{res}$ groups, respectively (Supplementary Table S1). As expected, we found several NE markers to be overrepresented in $Enti^{sens}$ cells, including synaptophysin (SYP), chromogranin A (CHGA), insulinoma-associated protein 1 (INSM1), and NEUROD1 as well as delta-like protein 3 (DLL3), which is regulated by the transcription factor ASCL1 (**Fig. 1C**; Supplementary Table S1). Of note, histone deacetylase 2 (HDAC2), along with HDAC 1 and 3, has recently been described to be selectively inhibited by entinostat. HDAC2 was significantly upregulated in $Enti^{sens}$ cells of our study (**Fig. 1C**, red dots; Supplementary Table S1). Besides the SCLC-Y marker YAP1, the $Enti^{res}$ group exhibited increased expression of several proteins associated with cancer aggressiveness and metastasis, including EGFR, ephrin type-A receptor 2 (EPHA2), signal transducer and activator of transcription 3 (STAT3), and caveolin 1/2 (CAV1/2; **Fig. 1C**, blue dots; Supplementary Table S1).

To further characterize the underlying proteomic profile affecting the response to entinostat, we conducted a 1D annotation enrichment analysis considering the KEGG database. Significantly overrepresented pathways in $Enti^{sens}$ cells encompassed various metabolic processes and molecular mechanisms including "DNA replication" and "Base excision repair" (**Fig. 1D**, red dots; Supplementary Table S1). Significant pathways in the $Enti^{res}$ group comprised the "Ras signaling pathway" and "Apoptosis," among others (**Fig. 1D**, blue dots; Supplementary Table S1). Furthermore, the KEGG pathways "Small cell lung cancer" and "Platinum drug resistance" emerged in $Enti^{res}$ cells (**Fig. 1D**; Supplementary Table S1). A summary of all dysregulated pathways in $Enti^{res}$ and $Enti^{sens}$ groups is listed in Supplementary Table S1.

Next, we compared our proteomic data with previously published sensitivity and resistance profiles of pan-HDAC inhibitors in SCLC. The comparison between the significant $Enti^{res}$ proteins and the resistant gene signature revealed 14 overlapping proteins (Supplementary Fig. S2A). We found that normalized log2 intensities of six proteins (RHOC, CAST, PLIN3, IQGAP1, ANXA, and LMN) correlated positively with entinostat IC_{50} values (Supplementary Fig. S2A). The two proteins INSM1 and HDAC2 overlapped in the $Enti^{sens}$ comparison, of which HDAC2 protein expression based on proteomics significantly correlates with entinostat IC_{50} values (Supplementary Fig. S2B).

Entinostat resistance correlates with cisplatin resistance

Next, we exposed the SCLC cell lines to cisplatin and calculated corresponding IC_{50} values ranging between 0.9 and 32.8 μmol/L

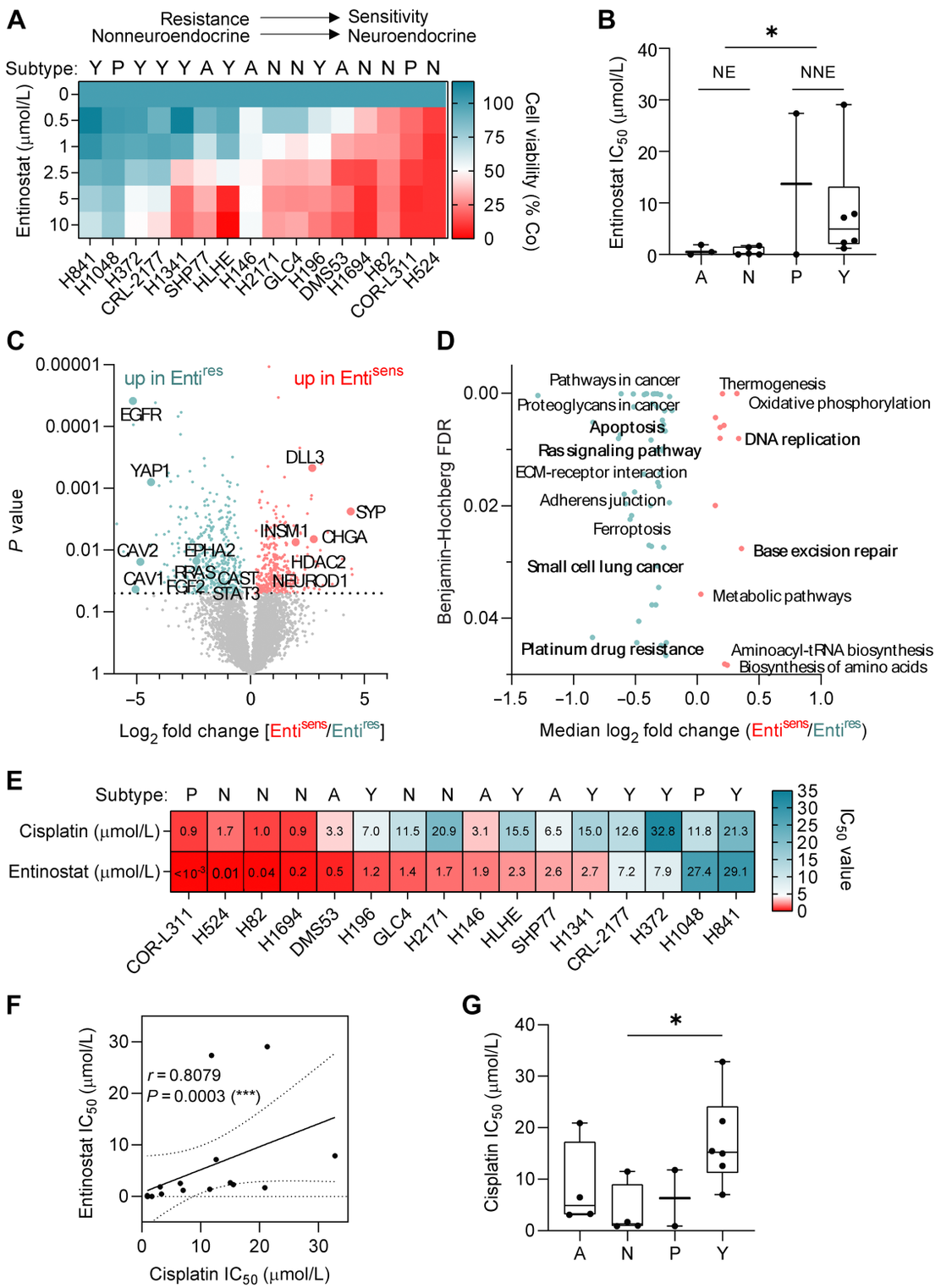

Figure 1.

Sensitivity to HDACi is associated with neuroendocrine features and cisplatin responsiveness in SCLC. **A,** Heat map depicting the percentage of viable cells (right Y-axis) after 72-hour treatment with entinostat at the indicated doses (left Y-axis). A: SCLC-A, P: SCLC-P, N: SCLC-N, Y: SCLC-Y. **B,** IC_{50} values for entinostat with respect to molecular subtypes. Each dot represents one cell line. NE: neuroendocrine, NNE: nonneuroendocrine, A: SCLC-A, P: SCLC-P, N: SCLC-N, Y: SCLC-Y. *t* test, *, $P < 0.05$. **C,** Significantly upregulated proteins in Enti^{sens} (red) and Enti^{res} (blue) cells. The dotted line indicates $P = 0.05$. **D,** Results from 1D annotation enrichment analysis show significantly overrepresented KEGG pathways in Enti^{sens} (red) and Enti^{res} (blue) cell lines. **E,** IC_{50} values of entinostat and cisplatin. A: SCLC-A, P: SCLC-P, N: SCLC-N, Y: SCLC-Y. **F,** Spearman correlation of entinostat and cisplatin IC_{50} values ($r = 0.8079$, $P = 0.0003$). Each dot represents one cell line. **G,** IC_{50} values were calculated from dose–response curves from cisplatin treatment for 72 hours. A: SCLC-A, P: SCLC-P, N: SCLC-N, Y: SCLC-Y. ANOVA with Dunn multiple comparisons tests; *, $P \leq 0.05$.

(**Fig. 1E**; Supplementary Fig. S3). Interestingly, we found a significant correlation between the IC_{50} values of cisplatin and entinostat, suggesting multidrug resistance in a predominantly YAP1-driven subset of SCLC cell lines (**Fig. 1F**). Regarding the molecular subtypes, cell lines from the NNE SCLC-Y subtype were more cisplatin-resistant (**Fig. 1G**), reflecting the resistance profile previously observed with entinostat (**Fig. 1B**).

Entinostat shows strong synergism with chemotherapy in chemoresistant SCLC cell lines

Based on the aforementioned results, we performed combination treatments with different doses of entinostat and cisplatin with all 16 cell lines (**Fig. 2A**; Supplementary Fig. S4). Synergistic, additive, or antagonistic drug interactions were assessed using the HSA model of the Combenefit software. Interestingly, we found diverging responses ranging from highly synergistic to weak antagonistic effects. These effects are portrayed in HSA synergy maps, whereas blue, green, and red colors indicate synergistic, additive, and antagonistic drug interactions, respectively (**Fig. 2B**; Supplementary Fig. S4B, S4D, and S4F).

In total, six cell lines displayed synergistic responses (SYN) by showing a corresponding maximum synergism score above 35, while the remainder demonstrated mostly additive to slightly synergistic effects (ADD; **Fig. 2C**). Importantly, all cell lines associated with synergistic effects were both cisplatin ($IC_{50} > 5$ μmol/L) and entinostat ($IC_{50} > 1$ μmol/L) resistant, suggesting a particularly strong synergism in chemoresistant SCLC cell lines. This finding was further supported by a significant correlation between the maximum synergism scores and the IC_{50} values for cisplatin and entinostat, respectively (**Fig. 2D**).

ICP-MS quantification of intracellular platinum (Pt) levels after 3-hour treatment with cisplatin alone or in combination with entinostat (pretreated for 24 hours) in four cell lines representative for the SYN and ADD groups (two per group, marked in blue and green in **Fig. 2C**) showed significantly higher Pt levels when combined with entinostat in all cell lines (**Fig. 2E**). Accordingly, both basal and combination Pt levels were significantly higher in the SYN group.

To assess whether the observed synergistic and additive effects with entinostat are specific to cisplatin, we performed multiple combination experiments with entinostat, carboplatin as another Pt compound, as well as etoposide, irinotecan, and epirubicin, which are all clinically relevant in SCLC. Strikingly, we observed a similar response pattern in all four representative cell lines with a mean maximum synergism score above and below 35 in cells from the SYN and ADD group in all drug combinations, respectively (**Fig. 2F**; Supplementary Fig. S5). We found a clear trend toward enhanced synergism in drug-resistant cells in the case of entinostat combined with epirubicin, irinotecan, and carboplatin (Supplementary Fig. S6). These data strongly support our previous findings that the combination of chemotherapy with entinostat is more effective in resistant SCLC cells.

Entinostat enhances the effects of cisplatin *in vivo*

To further validate our findings *in vivo*, the double-resistant cell line H841 with previously determined synergistic *in vitro* effects was injected subcutaneously into female SCID mice. After tumor formation, mice were treated via intraperitoneal injection of 3 mg/kg cisplatin once a week and received 25 mg/kg entinostat twice a week for 30 days. Entinostat treatment alone resulted in no difference in tumor size compared with the vehicle-treated control mice. Reduced tumor growth was observed in cisplatin-treated mice and to a higher extent in mice receiving combinational therapy as opposed to the control (**Fig. 3A**). Tumor weights were significantly different between the control and combination treatment groups (**Fig. 3B**). Also, the intratumoral Pt content was significantly higher in the combination group compared with the cisplatin-monotreatment group (**Fig. 3C**). Histologic analyses of the xenografts by TUNEL staining revealed significantly greater areas of necrosis (green) in the combination group compared with the control (**Fig. 3D** and **E**). Enhanced apoptosis was observed by evaluation of cleaved PARP expression in the nonnecrotic areas, showing significantly more positive cells in the combination group (vs. all other groups; **Fig. 3D** and **E**). Furthermore, the assessment of Ki67 indicated less cell proliferation in the entinostat and combination groups (**Fig. 3D** and **E**).

Proteomic evaluation suggests changes in cell cycle and DNA repair

In order to identify molecular differences between cell lines showing synergistic or additive effects upon combination treatment with entinostat and chemotherapy, we compared the previously defined SYN versus ADD cell panels using our proteomic data (according to their maximum synergism scores for entinostat/cisplatin we used all six cell lines from the SYN as well as the bottom six cell lines from the ADD group (**Fig. 2C**)). The list of significantly differentially expressed proteins between the two groups was subjected to ToppCluster analysis using the Hallmark gene set (33). Interestingly, the ADD group (green) was defined by dysregulation of "DNA Repair," "MYC Targets," and "PI3K–Akt–mTOR Signaling" (**Fig. 4A**; Supplementary Table S2). Additionally, a more strictly defined cell line panel ($N = 8$, top and bottom four cell lines, shown in **Fig. 2C**) was subjected to 1D annotation enrichment analysis using the KEGG database (**Fig. 4B**; Supplementary Table S2). Multiple DNA-repair processes such as NER, BER, and "DNA replication" were significantly higher in cell lines displaying additive effects (green). Additionally, the terms "oxidative phosphorylation," "DNA replication," and "cell-cycle" defined this group. On the contrary, multiple cellular pathways associated with cell plasticity including "ECM–receptor interaction," "focal adhesion," and "regulation of actin cytoskeleton" were overrepresented in cell lines showing synergistic features (**Fig. 4B**, blue; Supplementary Table S2).

Next, GSEA was performed, which confirmed previously reported dysregulation between SYN and ADD groups. SCLC cells with additive drug responses significantly overexpressed the gene panel associated with DNA repair (**Fig. 4C**) were indicated by normalized enrichment scores (NES) of 1.20. In contrast, genes defining epithelial-to-mesenchymal transition (EMT, NES = −1.16) or mediating apoptosis by activation of caspases (NES = −1.13) were enriched in cell lines where synergistic drug interactions occurred (**Fig. 4C**).

A representative panel of six cell lines for the ADD (CRL-2177, H1694, HLHE) and SYN (H372, H841, H2171) groups was defined for the following experiments, aiming to validate the mechanisms suggested by these data.

Entinostat levels are not affected by cisplatin

As described above, we found that cisplatin in combination with entinostat results in higher levels of intracellular/intratumoral amounts of Pt (**Figs. 2E** and **3C**). However, the increase was similar between SYN and ADD cell lines and did not explain the observed differential responses. Therefore, we next aimed to assess whether combination treatment results in different intracellular levels of entinostat and chose the acetylated Histone 3 (acetyl-H3) as a readout for entinostat efficacy. As expected, we found a dose-dependent increase in acetyl-H3 levels when cells were treated with entinostat alone (**Fig. 5A**, top). However, there was no further increase observed when various doses of cisplatin were added, suggesting no effect on

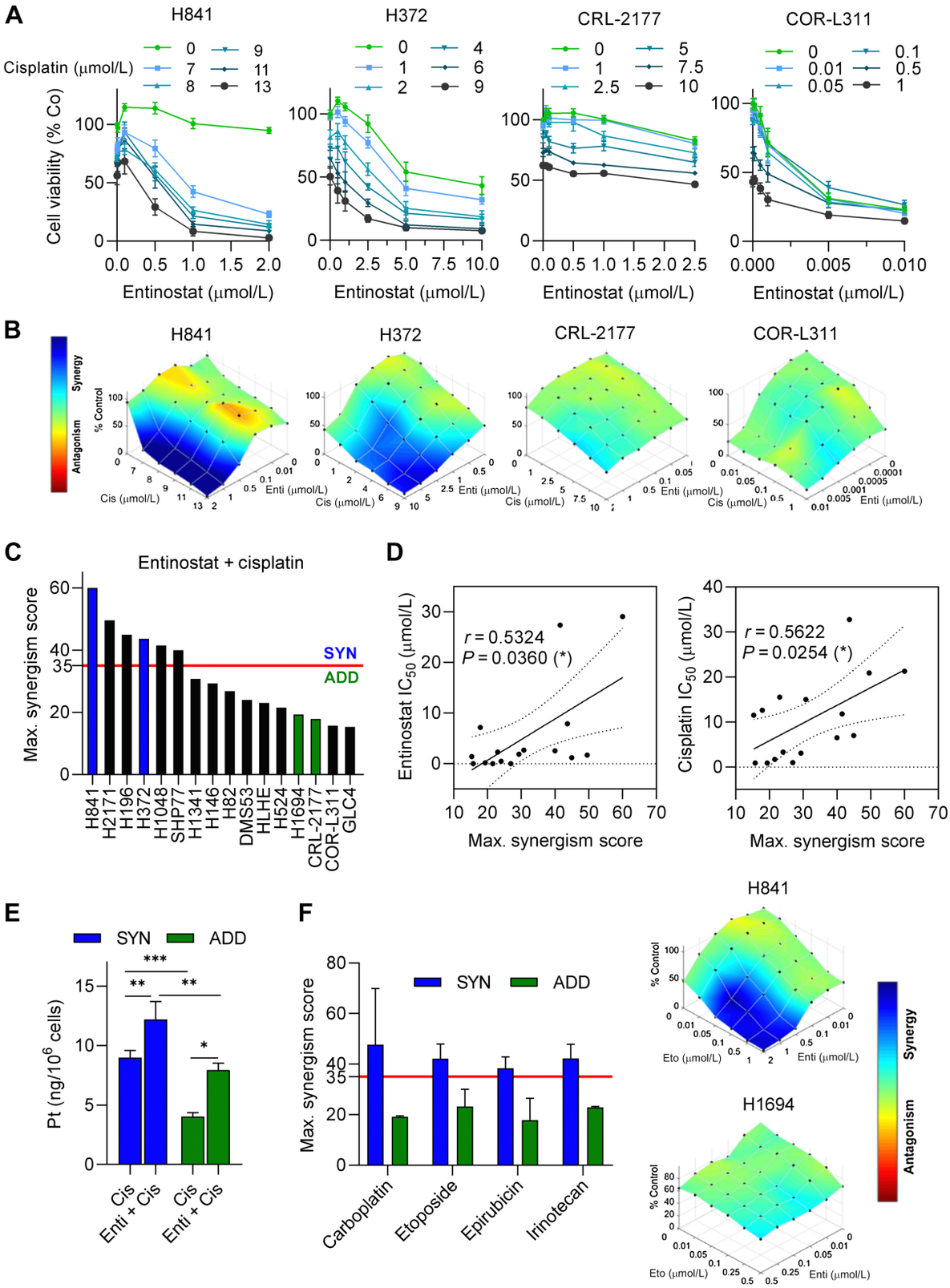

entinostat levels by cisplatin in the SYN or ADD group (**Fig. 5A**, middle). This was also reflected in a treatment setting containing the vehicle, entinostat alone, or in combination with cisplatin. Entinostat resulted in a strong increase in acetyl-H3 level; however, no superior increase with the combination was seen in either group (**Fig. 5A**, bottom).

Entinostat plus cisplatin leads to increased apoptosis in cells with synergistic responses

Next, we used flow cytometry and looked at cell death using AnnexinV and PI as markers for early apoptotic and dead cells. Double-positive cells were considered late apoptotic. Although no difference between the groups was found in the control cells, we observed significantly higher rates of apoptotic cells and cell death in the SYN cell panel in all treatments (**Fig. 5B**; Supplementary Fig. S7). Additionally, we performed immunoblots for cleaved PARP (cPARP; **Fig. 5C**). Pooled results showed that cells from the ADD group had slightly higher cPARP levels in all treatment groups. However, the highest levels were detected in the combination setting.

Combination of entinostat with cisplatin results in S-phase arrest and increases DNA damage in cells showing synergistic responses

Since the proteomic results indicated altered cell-cycle regulation, we also performed a FACS-based cell-cycle analysis (**Fig. 6A**). Similar cell-cycle distributions were observed with and without single treatments, with the majority of cells in the G_0–G_1 phase in the case of control and entinostat. Cisplatin-treated cells exhibited similar distributions in the G_0–G_1 phase and in the S-phase, respectively. Notably, combination therapy with entinostat and cisplatin resulted in a significant S-phase arrest in SYN compared with ADD cells, indicating increased DNA damage and higher repair activities in these cell lines (**Fig. 6A**; Supplementary Fig. S7).

Immunoblots for γH2AX as a marker for DNA damage demonstrated that γH2AX levels indeed peaked when the two agents were combined. However, when cell lines were pooled according to SYN and ADD responsiveness, no significant difference between the two groups was observed (**Fig. 6B**). Nevertheless, the results of comet assays, which reflect single- and double-strand breaks, showed significantly higher tail intensities in the cell lines with synergistic responses in untreated SYN and ADD groups, indicating higher levels of DNA damage in this group (**Fig. 6C**).

Cells showing additive effects are characterized by enhanced base excision repair

To further assess the DNA damage repair capacity of our cell line panel, we used an advanced SCGE approach. DNA damage was induced in A549 lung adenocarcinoma cells (RRID:CVCL_0023) by UVC exposure or Ro 19-8022 + Light to measure for nucleotide (NER) or base excision repair (BER), respectively. These cells were then incubated with lysates from untreated SCLC cells characterized by synergistic or additive responses to allow DNA repair by the present enzymes. In this assay, longer tail intensities are related to higher DNA-repair activity. Although there was no difference in NER, we found significantly higher BER activity in the ADD group (**Fig. 6D**; Supplementary Fig. S8). This represents a plausible explanation for the reduced DNA damage and for the high rate of apoptosis observed in experiments by entinostat and cisplatin in these cell lines.

Discussion

SCLC has been characterized by limited therapeutic innovation and lack of significant clinical breakthroughs for more than three decades. Further, SCLC was considered a homogeneous disease until recently, and the common standard-of-care therapy has been independent of the distinct molecular background or neuroendocrine features (2). Histone deacetylase inhibitors induce histone acetylation, resulting in altered gene-expression, cell-cycle progression, cell migration, and apoptosis. HDACis including entinostat (MS-275) have been demonstrated to be cytotoxic *in vitro* in multiple solid tumors including NSCLC and ovarian cancer (18, 34). Additionally, entinostat has been investigated in numerous phase I/II studies in melanoma as well as acute leukemia patients, resulting in moderate tolerability and long-term plateau of tumor growth (13, 14). However, the efficacy of HDACi monotherapy was limited due to its respective pleiotropic effects on cancer cells. Thus, its administration has been superseded through combination with cytotoxic agents because of a significant synergistic potential (35–37). Hence, we aimed to investigate the therapeutic efficacy of entinostat in a panel of human SCLC cell lines with respect to their molecular and NE specificities and dual therapy with relevant chemotherapeutic agents regarding SCLC.

In vitro studies in SCLC have already evaluated entinostat as a single agent among other HDACis such as vorinostat, belinostat, panobinostat, or apicidin (38). Results indicated a preferential response to HDAC inhibition in non-YAP1–driven subtypes. Of note, this is partly in line with our observation of significantly higher sensitivity in neuroendocrine SCLC subsets (SCLC-A/N) compared with nonneuroendocrine subtypes (SCLC-P/Y). The corresponding proteomic analysis identified differentially regulated proteins in $Enti^{sens}$ and $Enti^{res}$ SCLC cell lines including the transcription factor NEUROD1 and the notch inhibitory ligand DLL3, a direct transcriptional target of ASCL1 (39). These two lineage-defining transcription regulators of neuroendocrine differentiation (ASCL1 and NEUROD1) are both located in active chromatin regions encompassed within super-enhancers in SCLC cells (39–41). Such super-enhancers are commonly associated with enriched chromatin

Figure 2.

Entinostat synergizes with chemotherapy in the chemoresistant subset of SCLC cell lines *in vitro*. **A,** Dose–response curves after 72 hours of treatment with entinostat and cisplatin at indicated doses showed synergistic (H841 and H372) and additive (CRL-2177 and COR-L311) effects. Data, mean ± SEM of at least three experiments performed in triplicates. **B,** Corresponding HSA synergy maps, generated with the Combenefit software. Green areas indicate additive, blue areas highlight synergistic, and red areas show antagonistic drug interactions. **C,** Maximum synergism score derived from HSA analysis ranking all 16 cell lines from highly synergistic to additive. The red line (max. synergism score: 35) indicates the cutoff between SYN and ADD cells. **D,** Spearman correlation analysis of the maximum synergism score with entinostat and cisplatin, respectively. *, $P \le 0.05$. **E,** Pooled results of intracellular Pt measurements via ICP-MS of 2 cell lines per group (SYN: H841, H372; ADD: CRL-2177, H1694). Cells were treated with either cisplatin for 3 hours or pretreated with entinostat for 24 hours followed by 3 hours of cisplatin exposure. Data are shown as mean ± SEM of two experiments performed in triplicates. ANOVA and Sidak's multiple comparisons tests; *, $P \le 0.05$; **, $P < 0.01$; ***, $P < 0.001$. **F,** Pooled maximum synergism scores of entinostat in combination with carboplatin, etoposide, epirubicin, and irinotecan in SYN (blue = H841, H372) and ADD (green = CRL-2177, H1694) cells. Representative synergy maps of two representative cell lines treated with entinostat (Enti) and etoposide (Eto) were created with Combenefit.

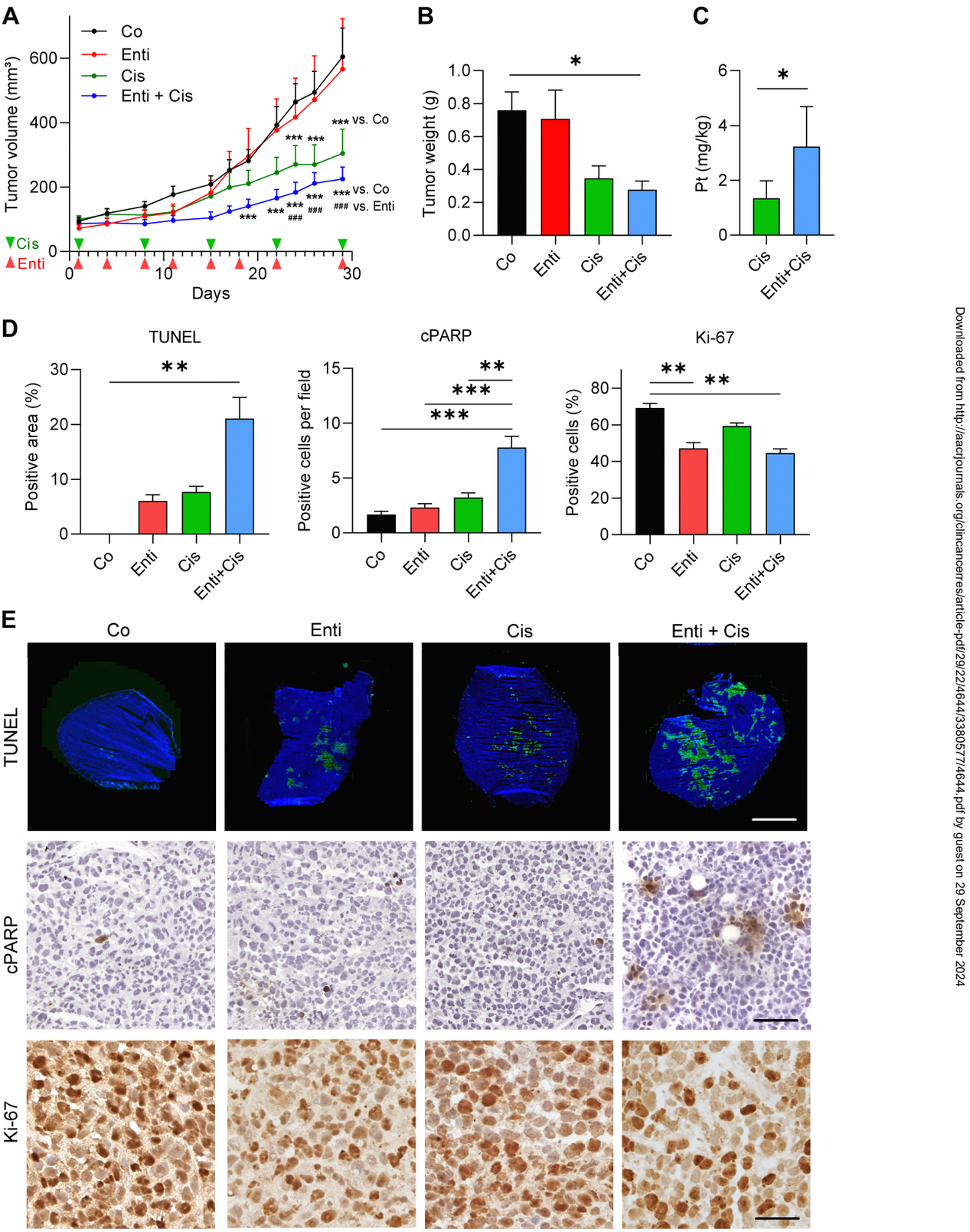

domains that are modified with acetylation of histone H3 lysine 27, resulting in active transcription (42).

It was recently reported that entinostat does not exclusively target HDAC1 and HDAC3 but also inhibits the deacetylation of HDAC2 (43). Here, we observed that HDAC2 was increased in entinostat-sensitive SCLC cell lines, indicating a potential predictive biomarker of entinostat responsiveness. Exome sequencing of primary and metastatic tumor samples obtained from research autopsies revealed clonal tumoral heterogeneity and identified resistance-associated truncal and subclonal alterations in relapsed SCLC, including alterations in the epigenetic modifiers CREBBP and HDAC2 (44). Along with *TP53* and *RB1* mutations, alterations of these two epigenetic regulators occur during early SCLC tumorigenesis (44). Altogether, these findings reinforce the hypothesis that cell lines featuring NE characteristics are more affected by HDAC inhibition.

In addition to the varying responses of SCLC cell lines to HDAC inhibition, we observed a strong positive correlation between entinostat and cisplatin resistance. Recently, belinostat was reported to display significant cross-resistance to multiple other HDAC inhibitors (45, 46). However, cross-resistance seen between HDACi and cytotoxic agents has not been described so far. Results from our pathway analysis indicated "platinum drug resistance" in Enti^{res} SCLC cell lines. In support of this, several research groups reported that HDACi enhance the cytotoxic activity of alkylating agents (21, 35, 36). Consequently, we tested the dual therapy using entinostat and chemotherapy in SCLC. Intriguingly, combinational treatment with entinostat and common chemotherapeutic agents, including cisplatin, carboplatin, and epirubicin, as well as the topoisomerase inhibitors irinotecan and etoposide resulted in synergistic effects in a subset of SCLC cell lines. Although synergistic drug interactions in *in vitro* studies have been previously described (47, 48), these calculations are based on a mathematical *in silico* HSA model. Therefore, further investigation is necessary to profoundly affirm the underlying modes of interaction between entinostat and chemotherapies in a more translational setting.

Intriguingly, the synergistic potential of combined therapy has been frequently observed in SCLC cell lines that showed cross-resistance between entinostat and cisplatin. Hence, combination approaches including HDAC inhibition and standard chemotherapy may offer a novel strategy to overcome chemoresistance in SCLC, which remains a major problem in the clinical management of this hard-to-treat disease (49). In SCLC, the combination of mocetinostat or vorinostat (HDACi) and topoisomerase inhibitors (topotecan or etoposide) have been described to improve synergistic drug interactions, especially when using sequential administration (50). Intriguingly, our mouse xenograft model confirmed the superior efficacy of DNA platination and HDAC inhibition, which resulted in tumor regression of a double-resistant SCLC cell line. This finding is in accordance with data from previous publications verifying the synergistic potential of HDACi and other chemotherapeutic agents (paclitaxel, trametinib) *in vivo* (51, 52). The dual PI3K–HDACi fimepinostat was recently reported to contribute to overcome platinum resistance in SCLC (53).

The initial hypothesis of increased cellular Pt uptake or decreased Pt efflux as the rationale behind synergistic drug response was not verified as all SCLC cell lines exhibited elevated Pt levels following combination treatment. Cisplatin is commonly eliminated from cancer cells via glutathione adduct formation. Enriched glutathione synthesis is highly associated with the overexpression of antiapoptotic proteins (54). However, apoptosis assays could not confirm differentially regulated pathways between SCLC cell lines associated with either synergistic or additive drug responses. Entinostat caused PARP cleavage in all cell lines; this has likewise been described in Hodgkin lymphoma cells in addition to synergistic drug interaction with Bcl-2 family inhibitors (55).

Human SCLC cells are highly associated with the biallelic loss of the tumor suppressors *TP53* and *RB1*, both of which are major modulators of the G_1–S transition of the cell cycle (56, 57). Altered expression results in the disruption of G_1–S checkpoint and cell-cycle arrest at the G_2–M phase with increased occurrence of DNA damage (58). In addition to these underlying molecular alterations in SCLC, cell-cycle distributions of SCLC cell lines upon entinostat single treatment led to an accumulation at the G_1 phase. Accordingly, entinostat treatment alone has been described to result in an accumulation of cells in the G_1 phase and a decrease in the S phase in B-cell lymphoma (59). Contrarily, cisplatin-treated SCLC cells were arrested in the S phase in our experiments; this is in line with observations in leukemia cells (60). However, the combined effect of entinostat and cisplatin in synergistic cells resulted in a shift from G_1 to S phase, further indicating the retention of the cells during synthesis. Of note, histone deacetylases 1 and 2 modulate the maintenance of S-phase chromatin (61). We hypothesize that prolonged synthesis may facilitate increased DNA platination. However, the exact mechanistic interactions between entinostat and cisplatin resulting in S-phase arrest remain to be elucidated.

When DNA damage occurs, cell-cycle checkpoints are activated, resulting in the retention of cells in G_1 (the G_1/S-phase checkpoint), delayed S phase (S-phase checkpoint), or prevented mitotic entry (the G_2–M-phase checkpoint). HDACis interfere with multiple DNA-repair processes and disrupt cell-cycle checkpoints (62). HDACi-induced histone hyperacetylation can cause structural alterations in chromatin, which also exposes parts of the DNA that are normally protected by heterochromatin to DNA-damaging agents including UV, radiation, cytotoxic drugs, or reactive oxygen species (63). Correspondingly, entinostat has been shown to potentiate the effect of radiation in combination with PD-1 inhibition in a murine lung cancer model (64) and FK228, an HDAC and PI3K inhibitor, has been demonstrated to act as radiosensitizer in SCLC (65).

In this study, we found that entinostat promotes the accumulation of the phosphorylated histone H2AX (γH2AX), an early marker of DNA double-strand breaks. Exposure of human lung adenocarcinoma, prostate, or renal carcinoma cells to vorinostat or entinostat has

Figure 3.

Entinostat and cisplatin synergize *in vivo* in a double-resistant SCLC cell line. **A,** Calculated tumor volumes over 30 days of treatment with vehicle (Co), entinostat (Enti), cisplatin (Cis), or a combination of both (Enti + Cis). Green and red arrows indicate days of cisplatin and entinostat treatment, respectively. Data are shown as mean ± SEM of 6–8 mice per group. Multiple *t* tests with Holm–Sidak correction, ***, $P < 0.001$ vs. Co, ###$P < 0.001$ vs. Enti. **B,** Tumor weight and (**C**) amount of intratumoral Pt measured by ICP-MS. ANOVA and Kruskal–Wallis multiple comparisons test in **B**, *t* test in **C**. *, $P \leq 0.05$. **D,** Quantification of TUNEL (green, nuclei: blue), cPARP, and Ki-67 (brown, nuclei: blue) in xenografts. Between 6 and 20 representative images were evaluated. ANOVA and Dunn multiple comparisons test; *, $P \leq 0.05$; **, $P < 0.01$; ***, $P < 0.001$. **E,** Representative images of xenografts used for evaluation. Scale bars, TUNEL: 2 mm, cPARP: 50 μm, Ki-67: 25 μm.

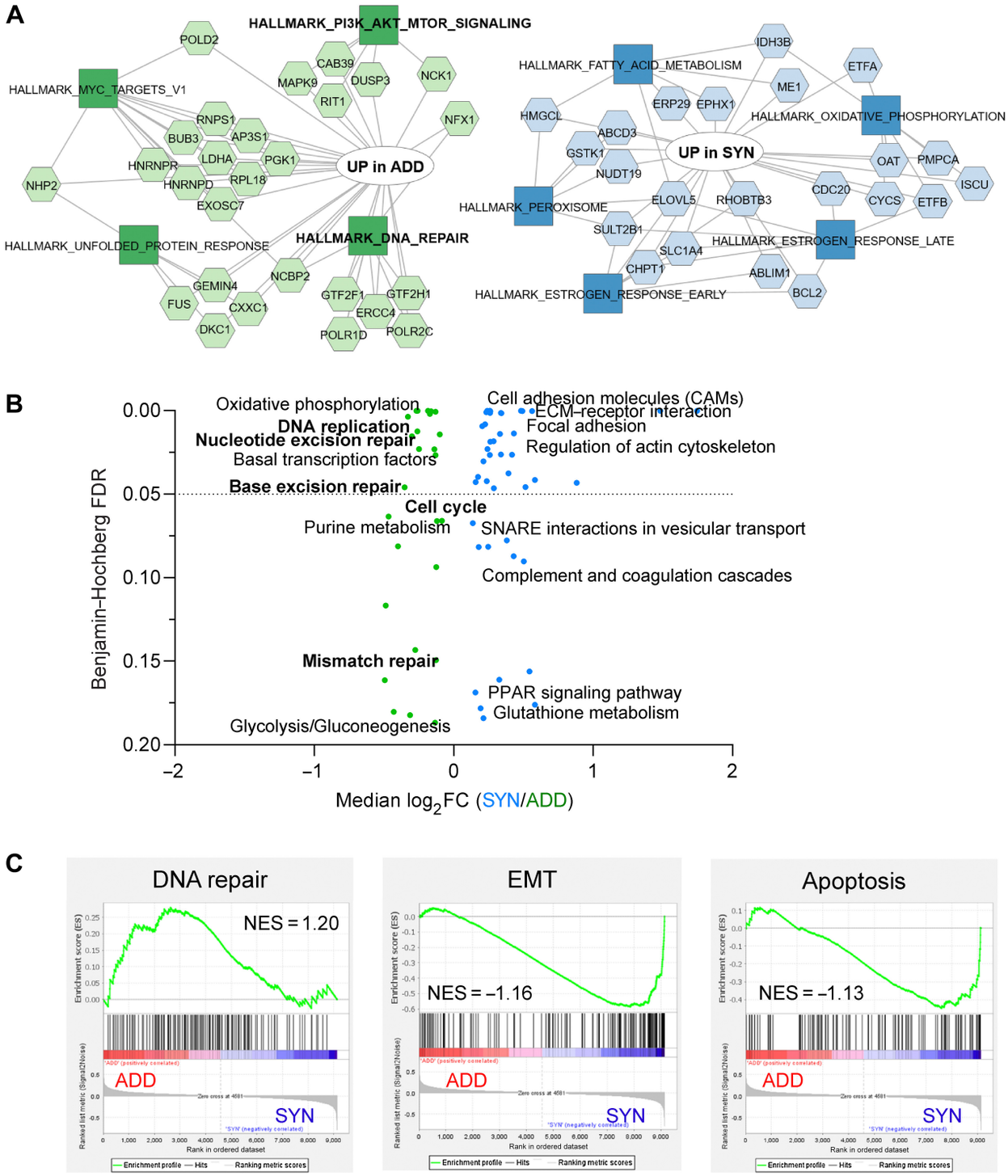

Figure 4.

Pathway analysis reveals alteration in cell-cycle and DNA damage repair. **A,** ToppCluster analysis of the differentially expressed proteins between the top six synergistic and bottom six additive cell lines according to the maximum synergism score shows associated hallmark gene sets within each group (blue: SYN; green: ADD). Gene sets with a *P* value cutoff of 0.05 using Bonferroni correction are depicted. **B,** 1D annotation enrichment analysis using KEGG pathways highlighting dysregulated pathways in SYN (blue) or ADD (green) cell lines. This analysis included a strict grouping of the top four synergistic and bottom four additive cell lines according to the maximum synergism score. The dotted line indicates the significance cutoff (FDR = 0.05). **C,** GSEA based on data from the strict grouping of SYN and ADD groups shows enrichment in DNA repair (ADD), EMT, and apoptosis (SYN). The Y-axis indicates the enrichment score (ES) and the x-axis shows identified genes (vertical black lines) represented in each pathway.

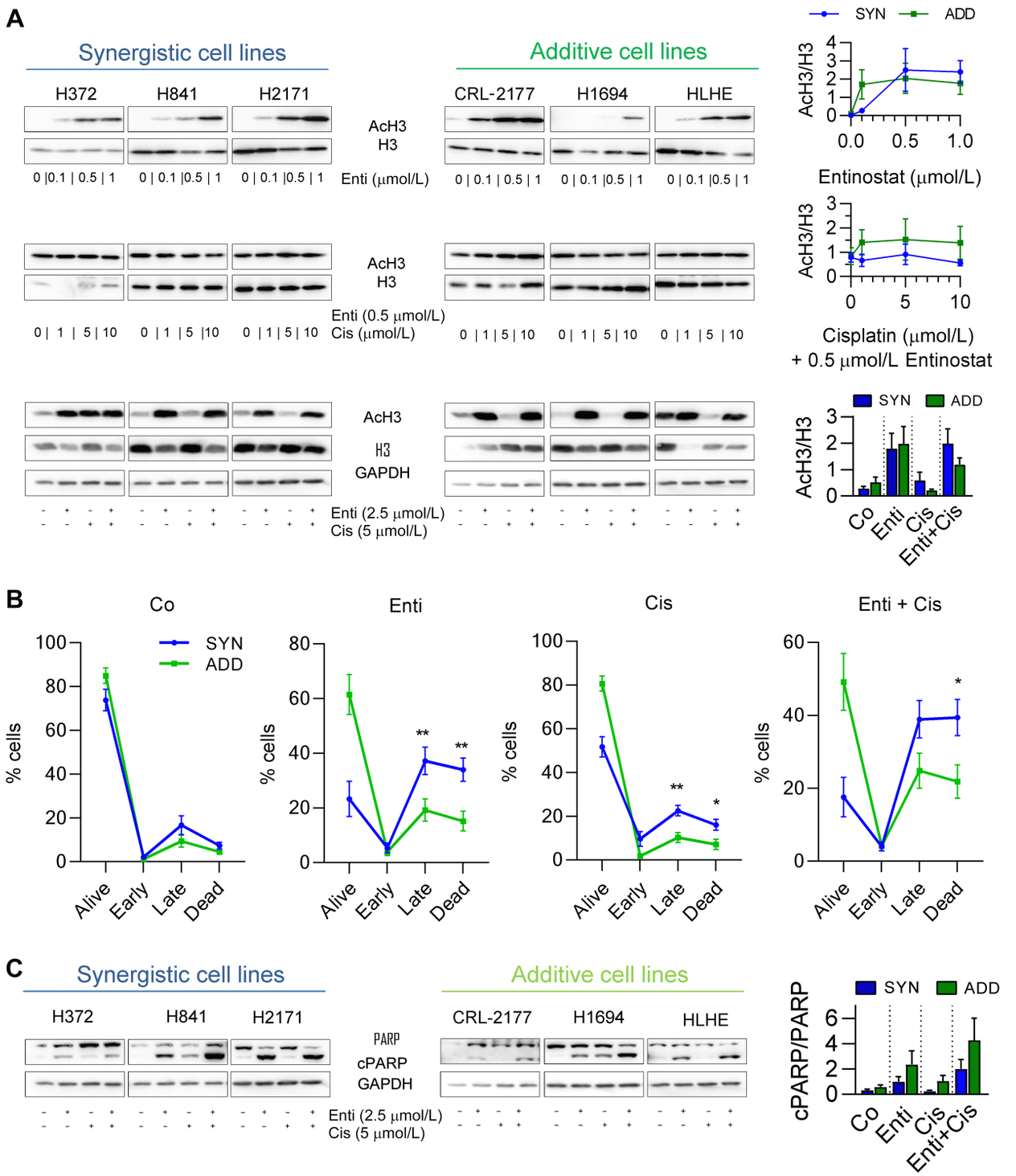

Figure 5.

Combination therapy of entinostat and cisplatin results in enhanced apoptosis in synergistic SCLC cell lines. **A,** Representative immunoblots of SYN/ADD cell line panels after 24 hours of treatment with entinostat (Enti) or cisplatin (Cis) at indicated doses. Densitometric quantification was performed using ImageJ of at least two repeats. AcH3 was normalized to H3 and the results are shown as the mean ± SEM. **B,** Flow cytometry-based apoptosis assay using Annexin V and propidium iodide (PI) staining after 48 hours of treatment with 2.5 μmol/L entinostat, 5 μmol/L cisplatin, a combination of both or solvent. Data, mean ± SEM of three repeats performed in triplicate of pooled results of three cell lines per group, respectively (blue, synergistic; green, additive). ANOVA and Sidak's multiple comparisons tests, *, $P \le 0.05$; **, $P < 0.01$; ***, $P < 0.001$. **C,** Representative immunoblots of SYN/ADD cell line panels after 24 hours of treatment with 2.5 μmol/L entinostat or 5 μmol/L cisplatin alone or in combination. cPARP was normalized to PARP, and the results shown are mean ± SEM. The same GAPDH lane is used in **A** and **C**; the same lysates were used to study different protein expressions and at least one of the proteins shown in each figure was detected on the same membrane.

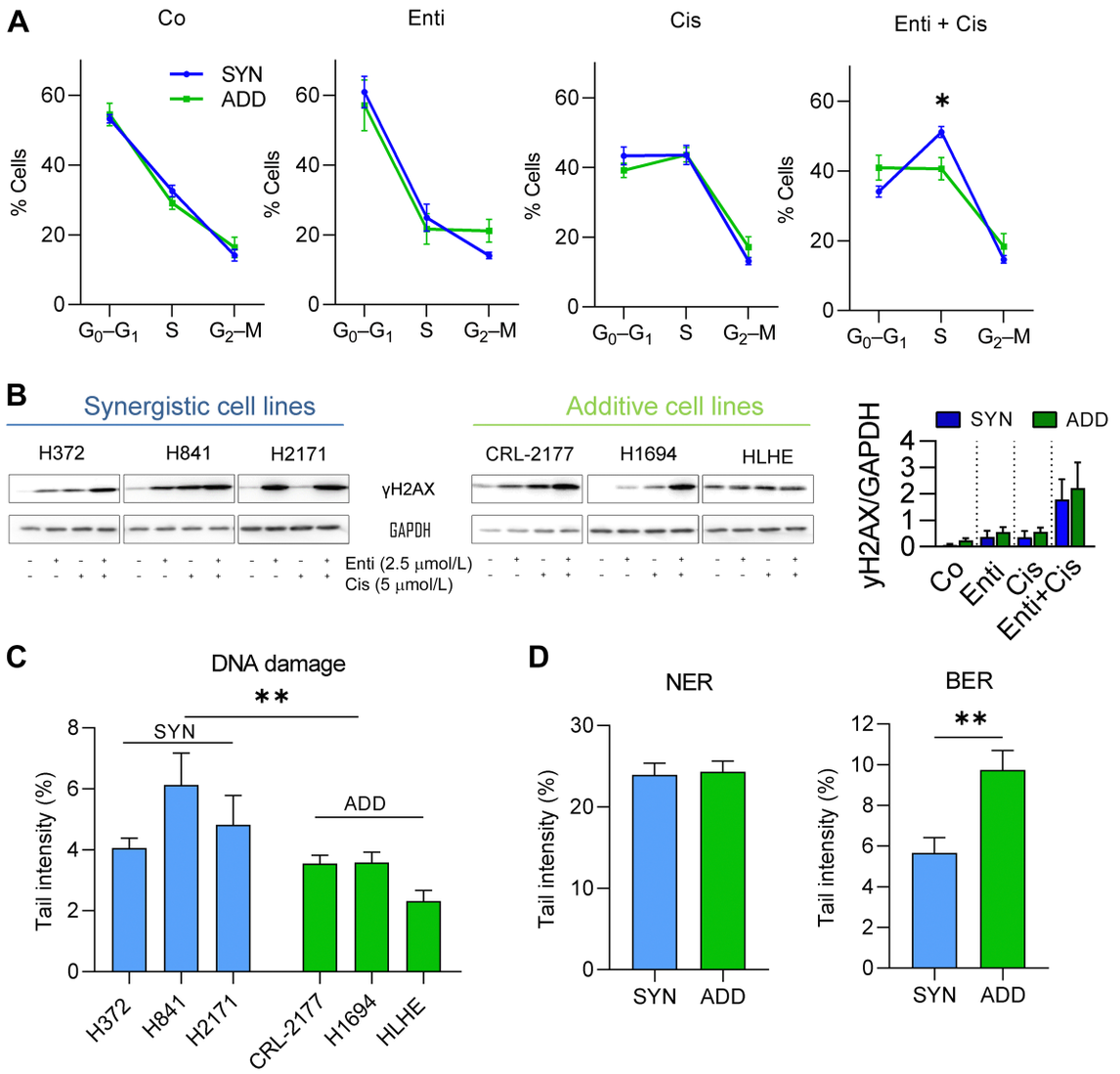

Figure 6.

Cell-cycle analysis indicates S-phase arrest and less BER capacity in SCLC cell lines related to synergistic responses upon combination therapy with entinostat and cisplatin. **A,** Cell-cycle distribution was analyzed via flow cytometry after 24 hours of treatment with respective IC_{50} values of each cell line (calculated after 72 hours). Experiments were performed in triplicate and data are shown as mean ± SEM of pooled results of three cell lines per group, respectively (blue, synergistic; green, additive). ANOVA and Sidak's multiple comparisons tests; *, $P \le 0.05$; **, $P < 0.01$; ***, $P < 0.001$. **B,** Representative immunoblots of SYN/ADD cell line panels after 24 hours of treatment with 2.5 μmol/L entinostat (Enti) or 5 μmol/L cisplatin (Cis) alone or in combination. Densitometric quantification was performed using ImageJ of at least 2 repeats. γH2AX was normalized to GAPDH and is shown as the mean ± SEM. The GAPDH lane is the same as in **Fig. 5A** and **5C**; the same lysates were used to study different protein expressions and at least one of the proteins shown in each figure was detected on the same membrane. **C,** Standard comet assay of SYN and ADD cell lines ($N = 3$, respectively) determined baseline DNA-damage levels, and data, mean ± SEM of at least two independent experiments. Mann–Whitney test; *, $P \le 0.05$; **, $P < 0.01$; ***, $P < 0.001$. **D,** Repair enzyme comet assay of pooled results (ADD or SYN cell lines, $N = 3$, respectively) elucidating the NER or BER capacity. Data, mean ± SEM of at least two independent experiments. Mann–Whitney test; *, $P \le 0.05$; **, $P < 0.01$; ***, $P < 0.001$.

yielded similar outcomes (66, 67). Moreover, these HDACi mediate the suppression of certain DNA-repair proteins in cancer cells, which may facilitate the failure of DNA double-strand break repair (63, 66, 67). Entinostat in combination with cisplatin demonstrated even higher levels of γH2AX in SCLC cell lines and proved to be superior to entinostat monotreatment.

We demonstrate the synergistic potential of dual entinostat and cisplatin therapy in SCLC cells to higher levels of baseline DNA damage in combination with decreased activity of BER. DNA-repair mechanisms such as BER are known to be involved in resistance to chemotherapy in a wide variety of cancer cells (68). BER is assumed to be mainly accomplished in the G_1 phase of the cell cycle by removing small base lesions and preparing DNA for subsequent replication (69). Similar to our findings, entinostat increased DNA tails in a dose- and time-dependent manner, indicating DNA damage in renal cancer cells (66).

Although the distinct genetic and proteomic landscape of SCLC molecular subtypes is becoming increasingly comprehensive, insights into underlying and considerable differences shaping differential responses to therapy remain to be elucidated. In the present study, we found that the HDACi entinostat is highly effective in SCLC cells with neuroendocrine characteristics. Additionally, our data show that resistant SCLC cells, specifically of nonneuroendocrine subtypes, are highly sensitive to a combined treatment with entinostat and cisplatin as well as other clinically relevant chemotherapeutic agents for SCLC. Furthermore, we identified reduced BER to be the driving molecular mechanism in cells showing superior effects to combination treatment, resulting in more therapy-induced DNA damage and cell death. Ultimately, further preclinical and clinical studies are warranted to investigate the effects of HDACi entinostat as a novel therapeutic option for SCLC.

Authors' Disclosures

Z. Megyesfalvi reports grants from the International Association for the Study of Lung Cancer, the Hungarian Academy of Sciences, and the Hungarian National Research, Development, and Innovation Office, and other support from the Ministry for Innovation and Technology of Hungary during the conduct of the study. C. Aigner reports grants from BMS, personal fees and nonfinancial support from MSD, personal fees from Roche, and grants and personal fees from AstraZeneca and Ewimed outside the submitted work. B. Dome reports grants from the Austrian Science Fund and the Hungarian National Research, Development, and Innovation Office during the conduct of the study. No disclosures were reported by the other authors.

Authors' Contributions

A. Solta: Conceptualization, data curation, formal analysis, validation, investigation, visualization, methodology, writing–original draft, writing–review and editing. **K. Boettiger:** Methodology, writing–review and editing. **I. Kovács:** Methodology, writing–original draft. **C. Lang:** Writing–original draft. **Z. Megyesfalvi:** Writing–review and editing. **F. Ferk:** Methodology. **M. Mišík:** Methodology. **K. Hoetzenecker:** Writing–review and editing. **C. Aigner:** Writing–review and editing. **C.R. Kowol:** Methodology, writing–review and editing. **S. Knasmueller:** Methodology, writing–review and editing. **M. Grusch:** Writing–review and editing. **B. Szeitz:** Formal analysis, methodology. **M. Rezeli:** Formal analysis, methodology, writing–review and editing. **B. Dome:** Supervision, writing–review and editing. **K. Schelch:** Conceptualization, supervision, validation, methodology, project administration.

Acknowledgments

We thank Barbara Dekan, Gerhard Zeitler, and Julia Zoller for technical assistance with cell culture and ICP-MS measurements. We also thank Gerald Timelthaler for his help with imaging and analysis. K. Schelch was supported by the Austrian Science Fund (FWF No. T 1062-B33). B. Dome was supported by the Austrian Science Fund (FWF I3522, FWF I3977, and I4677). B. Dome and Z. Megyesfalvi acknowledge funding from the Hungarian National Research, Development and Innovation Office (KH130356 and KKP126790 to B. Dome; 2020-1.1.6-JÖVŐ and TKP2021-EGA-33 to B. Dome and Z. Megyesfalvi). Z. Megyesfalvi was supported by the Hungarian Respiratory Society (MPA #2020), by the UNKP-20-3 and UNKP-21-3 New National Excellence Program of the Ministry for Innovation and Technology of Hungary, and by the Bolyai Research Scholarship of the Hungarian Academy of Sciences. Z. Megyesfalvi is also a recipient of the IASLC/ILCF Young Investigator Grant 2022. MR acknowledges funding from the Mrs. Berta Kamprad's Cancer Foundation (FBKS-2020-22-(291)). M. Rezeli was supported by the City of Vienna Fund for Innovative Interdisciplinary Cancer Research (No. 21132). B. Szeitz was supported by the Semmelweis 250+ Excellence PhD Scholarship (EFOP-3.6.3-VEKOP-16-2017-00009) and the ÚNKP-22-3-II New National Excellence Program of the Ministry for Culture and Innovation from the source of the National Research, Development and Innovation Fund.

The publication costs of this article were defrayed in part by the payment of publication fees. Therefore, and solely to indicate this fact, this article is hereby marked "advertisement" in accordance with 18 USC section 1734.

Note

Supplementary data for this article are available at Clinical Cancer Research Online (http://clincancerres.aacrjournals.org/).

Received June 20, 2023; revised August 10, 2023; accepted September 13, 2023; published first September 19, 2023.

References

1. Rudin CM, Brambilla E, Faivre-Finn C, Sage J. Small-cell lung cancer. Nat Rev Dis Prim 2021;7:3.
2. Schwendenwein A, Megyesfalvi Z, Barany N, Valko Z, Bugyik E, Lang C, et al. Molecular profiles of small cell lung cancer subtypes: therapeutic implications. Mol. Ther. -Oncolytics. 2021;20:470–83.
3. Inoue M, Sawabata N, Okumura M. Surgical intervention for small-cell lung cancer: what is the surgical role?. Gen. Thorac. Cardiovasc. Surg 2012;60:401–5.
4. Alexandrov LB, Ju YS, Haase K, Van Loo P, Martincorena I, Nik-Zainal S, et al. Mutational signatures associated with tobacco smoking in human cancer. Science 2016;354:618–22.
5. Rudin CM, Poirier JT, Byers LA, Dive C, Dowlati A, George J, et al. Molecular subtypes of small cell lung cancer: a synthesis of human and mouse model data. Nat Rev Cancer 2019;19:289–97.
6. Evans WK, Osoba D, Feld R, Shepherd FA, Bazos MJ, DeBoer G. Etoposide (VP-16) and cisplatin: An effective treatment for relapse in small-cell lung cancer. J Clin Oncol 1985;3:65–71.
7. Green RA, Humphrey E, Close H, Patno ME. Alkylating agents in bronchogenic carcinoma. Am J Med 1969;46:516–25.
8. Fee WH, Farber MO, Livingston RB, Gottlieb JA. Improved chemotherapy for small-cell undifferentiated lung cancer. JAMA 1976;235:1225–9.
9. Rossi A, Di Maio M, Chiodini P, Rudd RM, Okamoto H, Skarlos DV, et al. Carboplatin- or cisplatin-based chemotherapy in first-line treatment of small-cell lung cancer: The COCIS meta-analysis of individual patient data. J Clin Oncol 2012;30:1692–8.
10. Annic J, Babey H, Corre R, Descourt R, Quéré G, Renaud E, et al. Real-life second-line epirubicin-paclitaxel regimen as treatment of relapsed small-cell lung cancer: EpiTax study. Cancer Med 2023;12:2658–65.
11. Zhang C, Leighl NB, Wu YL, Zhong WZ. Emerging therapies for small cell lung cancer. J Hematol Oncol 2019;12:1–11.
12. Sabari JK, Lok BH, Laird JH, Poirier JT, Rudin CM. Unravelling the biology of SCLC: implications for therapy. Nat Rev Clin Oncol 2017;14:549–61.
13. Hauschild A, Trefzer U, Garbe C, Kaehler KC, Ugurel S, Kiecker F, et al. Multicenter phase II trial of the histone deacetylase inhibitor pyridylmethyl-N-{4-[(2-aminophenyl)-carbamoyl]-benzyl}-carbamate in pretreated metastatic melanoma. Melanoma Res 2008;18:274–8.
14. Gojo I, Jiemjit A, Trepel JB, Sparreboom A, Figg WD, Rollins S, et al. Phase 1 and pharmacologic study of MS-275, a histone deacetylase inhibitor, in adults with refractory and relapsed acute leukemias. Blood 2007;109:2781–90.
15. Sun L, He Q, Tsai C, Lei J, Chen J, Makcey LV, et al. HDAC inhibitors suppressed small cell lung cancer cell growth and enhanced the suppressive effects of receptor-targeting cytotoxins via upregulating somatostatin receptor II. Am J Transl Res 2018;10:545–53.
16. Bondarev AD, Attwood MM, Jonsson J, Chubarev VN, Tarasov VV, Schiöth HB. Recent developments of HDAC inhibitors: emerging indications and novel molecules. Br J Clin Pharmacol 2021;87:4577–97.
17. Connolly RM, Rudek MA, Piekarz R. Entinostat: a promising treatment option for patients with advanced breast cancer. Futur Oncol 2017;13:1137.
18. Mamdani H, Jalal SI. Histone deacetylase inhibition in non-small cell lung cancer: hype or hope?. Front. Cell Dev. Biol 2020;8:582370.
19. Calzetta L, Koziol-White C. Pharmacological interactions: Synergism, or not synergism, that is the question. Curr Res Pharmacol drug Discov 2021;2:100046.
20. Hontecillas-Prieto L, Flores-Campos R, Silver A, de Álava E, Hajji N, García-Domínguez DJ. Synergistic enhancement of cancer therapy using HDAC inhibitors: opportunity for clinical trials. Front. Genet 2020;11:578011.

21. Witta SE, Chan D, Girard L, Zheng D, Franekova V, Peyton M, et al. Effects of entinostat on resistance to cetuximab and EGFR TKIs in non-small cell lung cancer. J Clin Oncol 2012;30:e18077–. Available from: http://ascopubs.org/doi/10.1200/jco.2012.30.15_suppl.e18077
22. Wang C, Hamacher A, Petzsch P, Köhrer K, Niegisch G, Hoffmann MJ, et al. Combination of decitabine and entinostat synergistically inhibits urothelial bladder cancer cells via activation of FoxO1. Cancers (Basel) 2020;12:337.
23. Szeitz B, Megyesfalvi Z, Woldmar N, Valkó Z, Schwendenwein A, Bárány N, et al. In-depth proteomic analysis reveals unique subtype-specific signatures in human small-cell lung cancer. Clin Transl Med 2022;12:e1060.
24. Cox J, Mann M. 1D and 2D annotation enrichment: a statistical method integrating quantitative proteomics with complementary high-throughput data. BMC Bioinf 2012;13 Suppl 1:S12. Available from: http://www.biomedcentral.com/1471–2105/13/S16/S12
25. Subramanian A, Tamayo P, Mootha VK, Mukherjee S, Ebert BL, Gillette MA, et al. Gene set enrichment analysis: a knowledge-based approach for interpreting genome-wide expression profiles. Proc Natl Acad Sci USA 2005;102:15545–50.
26. Mootha VK, Lindgren CM, Eriksson K-F, Subramanian A, Sihag S, Lehar J, et al. PGC-1α-responsive genes involved in oxidative phosphorylation are coordinately downregulated in human diabetes. Nat Genet 2003;34:267–73.
27. Azqueta A, Muruzabal D, Boutet-Robinet E, Milic M, Dusinska M, Brunborg G, et al. Technical recommendations to perform the alkaline standard and enzyme-modified comet assay in human biomonitoring studies. Mutat Res Genet Toxicol Environ Mutagen 2019;843:24–32.
28. Azqueta A, Langie SAS, Slyskova J, Collins AR. Measurement of DNA base and nucleotide excision repair activities in mammalian cells and tissues using the comet assay: a methodological overview. DNA Repair (Amst) 2013;12:1007–10.
29. Vodenkova S, Azqueta A, Collins A, Dusinska M, Gaivão I, Møller P, et al. An optimized comet-based in vitro DNA repair assay to assess base and nucleotide excision repair activity. Nat Protoc 2020;15:3844–78.
30. Team RC. A language and environment for statistical computing. R Foundation for Statistical Computing 2021. Available from: https://www.r-project.org/. 2021
31. Tyanova S, Temu T, Sinitcyn P, Carlson A, Hein MY, Geiger T, et al. The Perseus computational platform for comprehensive analysis of (prote)omics data. Nat Methods 2016;13:731–40.
32. Di Veroli GY, Fornari C, Wang D, Mollard S, Bramhall JL, Richards FM, et al. Combenefit: An interactive platform for the analysis and visualization of drug combinations. Bioinformatics 2016;32:2866–8.
33. Liberzon A, Birger C, Thorvaldsdóttir H, Ghandi M, Mesirov JP, Tamayo P. The molecular signatures database hallmark gene set collection. Cell Syst 2015;1:417–25.
34. Bandolik JJ, Hamacher A, Schrenk C, Weishaupt R, Kassack MU. Class i-histone deacetylase (Hdac) inhibition is superior to pan-hdac inhibition in modulating cisplatin potency in high-grade serous ovarian cancer cell lines. Int J Mol Sci 2019;20:3052.
35. Tang SW, Thomas A, Murai J, Trepel JB, Bates SE, Rajapakse VN, et al. Overcoming resistance to DNA-targeted agents by epigenetic activation of schlafen 11 (SLFN11) expression with class I histone deacetylase inhibitors. Clin Cancer Res 2018;24:1944–53.
36. Vendetti FP, Topper M, Huang P, Dobromilskaya I, Easwaran H, Wrangle J, et al. Evaluation of azacitidine and entinostat as sensitization agents to cytotoxic chemotherapy in preclinical models of non-small cell lung cancer. Oncotarget 2015;6:56–70.
37. Huang YH, Klingbeil O, He XY, Wu XS, Arun G, Lu B, et al. POU2F3 is a master regulator of a tuft cell-like variant of small cell lung cancer. Genes Dev 2018;32:915–28.
38. Yang H, Sun B, Xu K, He Y, Zhang T, Hall SRR, et al. Pharmaco-transcriptomic correlation analysis reveals novel responsive signatures to HDAC inhibitors and identifies Dasatinib as a synergistic interactor in small-cell lung cancer. eBioMedicine 2021;69:103457.
39. Borromeo MD, Savage TK, Kollipara RK, He M, Augustyn A, Osborne JK, et al. ASCL1 and NEUROD1 reveal heterogeneity in pulmonary neuroendocrine tumors and regulate distinct genetic programs. Cell Rep 2016;16:1259–72.
40. Christensen CL, Kwiatkowski N, Abraham BJ, Carretero J, Al-Shahrour F, Zhang T, et al. Targeting transcriptional addictions in small cell lung cancer with a covalent CDK7 inhibitor. Cancer Cell 2014;26:909–22.
41. Pongor LS, Schultz CW, Rinaldi L, Wangsa D, Redon CE, Takahashi N, et al. Extrachromosomal DNA amplification contributes to small cell lung cancer heterogeneity and is associated with worse outcomes. Cancer Discov 2023;13:928–49.
42. Gazdar AF, Bunn PA, Minna JD. Small-cell lung cancer: what we know, what we need to know and the path forward. Nat Rev Cancer 2017;17:725–37.
43. Liu B, Chen S, Rose AL, Chen D, Cao F, Zwinderman M, et al. Inhibition of histone deacetylase 1 (HDAC1) and HDAC2 enhances CRISPR/Cas9 genome editing. Nucleic Acids Res 2020;48:517–32.
44. Chen H-Z, Bonneville R, Paruchuri A, Reeser JW, Wing MR, Samorodnitsky E, et al. Genomic and transcriptomic characterization of relapsed SCLC through rapid research autopsy. JTO Clin Res reports 2021;2:100164.
45. Islam S, Espitia CM, Persky DO, Carew JS, Nawrocki ST. Resistance to histone deacetylase inhibitors confers hypersensitivity to oncolytic reovirus therapy. Blood Adv 2020;4:5297–310.
46. Dedes KJ, Dedes I, Imesch P, von Bueren AO, Fink D, Fedier A. Acquired vorinostat resistance shows partial cross-resistance to 'second-generation' HDAC inhibitors and correlates with loss of histone acetylation and apoptosis but not with altered HDAC and HAT activities. Anticancer Drugs 2009;20:321–33.
47. Valko Z, Megyesfalvi Z, Schwendenwein A, Lang C, Paku S, Barany N, et al. Dual targeting of BCL-2 and MCL-1 in the presence of BAX breaks venetoclax resistance in human small cell lung cancer. Br J Cancer 2023;128:1850–61.
48. Schelch K, Hoda MA, Klikovits T, Münzker J, Ghanim B, Wagner C, et al. Fibroblast growth factor receptor inhibition is active against mesothelioma and synergizes with radio- and chemotherapy. Am J Respir Crit Care Med 2014;190:763–72.
49. Megyesfalvi Z, Gay CM, Popper H, Pirker R, Ostoros G, Heeke S, et al. Clinical insights into small cell lung cancer: tumor heterogeneity, diagnosis, therapy, and future directions. CA Cancer J Clin 2023. doi: 10.3322/caac.21785
50. Gray J, Cubitt CL, Zhang S, Chiappori A. Combination of HDAC and topoisomerase inhibitors in small cell lung cancer. Cancer Biol Ther 2012;13:614–22.
51. Faião-Flores F, Emmons MF, Durante MA, Kinose F, Saha B, Fang B, et al. HDAC inhibition enhances the in vivo efficacy of MEK inhibitor therapy in uveal melanoma. Clin Cancer Res 2019;25:5686–701.
52. Zuco V, de Cesare M, Cincinelli R, Nannei R, Pisano C, Zaffaroni N, et al. Synergistic antitumor effects of novel HDAC inhibitors and paclitaxel in vitro and in vivo. PLoS One 2011;6:e29085.
53. Chen J, Guanizo AC, Jakasekara WSN, Inampudi C, Luong Q, Garama DJ, et al. MYC drives platinum resistant SCLC that is overcome by the dual PI3K-HDAC inhibitor fimepinostat. J Exp Clin Cancer Res 2023;42:100.
54. Jin KL, Park J-Y, Noh EJ, Hoe KL, Lee JH, Kim J-H, et al. The effect of combined treatment with cisplatin and histone deacetylase inhibitors on HeLa cells. J Gynecol Oncol 2010;21:262–8.
55. Jóna A, Khaskhely N, Buglio D, Shafer JA, Derenzini E, Bollard CM, et al. The histone deacetylase inhibitor entinostat (SNDX-275) induces apoptosis in Hodgkin lymphoma cells and synergizes with Bcl-2 family inhibitors. Exp Hematol 2011;39:1007–1017.
56. Pavan A, Attili I, Pasello G, Guarneri V, Conte PF, Bonanno L. Immunotherapy in small-cell lung cancer: from molecular promises to clinical challenges. J. Immunother 2019;7:205.
57. George J, Lim JS, Jang SJ, Cun Y, Ozretić L, Kong G, et al. Comprehensive genomic profiles of small cell lung cancer. Nature 2015;524:47–53.
58. Sen T, Gay CM, Byers LA. Targeting DNA damage repair in small cell lung cancer and the biomarker landscape. Transl Lung Cancer Res 2018;7:50–68.
59. Frys S, Simons Z, Hu Q, Barth MJ, Gu JJ, Mavis C, et al. Entinostat, a novel histone deacetylase inhibitor is active in B-cell lymphoma and enhances the anti-tumour activity of rituximab and chemotherapy agents. Br J Haematol 2015;169:506–19.
60. Velma V, Dasari SR, Tchounwou PB. Low doses of cisplatin induce gene alterations, cell cycle arrest, and apoptosis in human promyelocytic leukemia cells. Biomark Insights 2016;11:113–21.
61. Bhaskara S, Jacques V, Rusche JR, Olson EN, Cairns BR, Chandrasekharan MB. Histone deacetylases 1 and 2 maintain S-phase chromatin and DNA replication fork progression. Epigenetics Chromatin 2013;6:27.
62. Bose P, Dai Y, Grant S. Histone deacetylase inhibitor (HDACI) mechanisms of action: emerging insights. Pharmacol Ther 2014;143:323–36.
63. Lee J-H, Choy ML, Ngo L, Foster SS, Marks PA. Histone deacetylase inhibitor induces DNA damage, which normal but not transformed cells can repair. Proc Natl Acad Sci USA 2010;107:14639–44.
64. Kim Y, Park K, Kim YJ, Shin SW, Kim YJ, Choi C, et al. Immunomodulation of HDAC inhibitor entinostat potentiates the anticancer effects of radiation and PD-1 blockade in the murine Lewis lung carcinoma model. Int J Mol Sci 2022;23:15539.

65. Li H, Ma L, Bian X, Lv Y, Lin W. FK228 sensitizes radioresistant small cell lung cancer cells to radiation. Clin Epigenetics 2021; 13:41.
66. Kiweler N, Wünsch D, Wirth M, Mahendrarajah N, Schneider G, Stauber RH, et al. Histone deacetylase inhibitors dysregulate DNA repair proteins and antagonize metastasis-associated processes. J Cancer Res Clin Oncol 2020; 146:343.
67. Pan CH, Chang YF, Lee MS, Wen BC, Ko JC, Liang SK, et al. Vorinostat enhances the cisplatin-mediated anticancer effects in small cell lung cancer cells. BMC Cancer 2016;16:857.
68. Li LY, GY Di, Chen XS, Yang JM, Cheng Y. DNA repair pathways in cancer therapy and resistance. Front Pharmacol 2020;11:629266
69. Dianov GL, Hübscher U. Mammalian base excision repair: the forgotten archangel. Nucleic Acids Res 2013;41:3483–90.